Ranges and Stopping Cross Sections of Low-Energy Tritons*

R. L. WOLKE
Wherrett Laboratory of Nuclear Chemistry, University of Pittsburgh, Pittsburgh, Pennsylvania† and Department of Chemistry, University of Florida, Gainesville, Florida

W. N. BISHOP‡
Department of Chemistry, University of Florida, Gainesville, Florida

AND

E. EICHLER, N. R. JOHNSON, AND G. D. O'KELLEY
Chemistry Division, Oak Ridge National Laboratory,|| Oak Ridge, Tennessee

(Received 16 October 1962)

Stopping cross sections and ranges of tritons as a function of energy from ~0.2 to 2.7 MeV have been measured in polystyrene, nitrogen, air, aluminum, argon, nickel, krypton, and xenon by a conicidence technique utilizing the $Li^6(n,\alpha)H^3$ reaction. The ranges found for 2.736-MeV tritons in these materials are 6.12±0.10, 7.26±0.06, 7.34±0.06, 10.10±0.10, 11.40±0.09, 15.15±0.15, 17.83±0.18, and 20.36±0.20 mg/cm², respectively. Above $E_t/Z \approx 0.05$, the atomic stopping cross section ϵ in eV-cm² is given by $\epsilon \times 10^{15} = 4(E_t/Z)^{-1/2} - (E_t/Z)^{1/2}$, where E_t is the triton energy in MeV and Z is the atomic number of the absorber. The data are compared with stopping theories for the velocity region in which shell effects cause deviations from the simple higher energy stopping theory.

I. INTRODUCTION

THE stopping of heavy charged particles in matter is well understood provided that the particle velocity is large compared with (1) the ground-state orbital velocity of its own atomic electrons and (2) the velocities of the most energetic atomic electrons in the stopping atoms. Theoretical treatments[1-3] using both of these simplifying assumptions have been extremely successful in predicting and reproducing experimental energy-loss data for heavy, charged particles. If, as is usually the case, the particles are of lower Z than the stopping medium, the satisfaction of condition 2 requires a higher velocity than the satisfaction of condition 1, so that as the particle slows down its velocity first fails to exceed that of some of the stopping electrons and the particle enters what we call the "velocity region II." When the particle velocity has been reduced to a few times the velocity of its own electrons, its average charge is decreased by electron pickup, and it enters what we call the "velocity region I."

While only exploratory theoretical work[4] has yet been done in velocity region I because of the difficulty of calculating the energy loss of neutralized particles, significant progress has been made in region II by the calculation of "shell correction" terms to the basic theory[1] for the reduction in stopping power when the velocities of the K,[2,5] L,[6] and higher[7] orbital electrons of the stopping medium are not exceeded by the particle. Some success was also attained by a treatment due to Lindhard and Scharff[8] which replaces the logarithmic term in the Bethe energy-loss equation,[1,2]

$$-dE/dx = (4\pi z^2 e^4 NZ/m_0 v^2) \ln(2m_0 v^2/I), \quad (1)$$

by a dimensionless function L of the single variable $x = v^2/(v_0^2 Z)$, which arises from the Fermi-Thomas model. Thus,

$$-\frac{dE}{dx}\Big/N = \epsilon = \frac{4\pi z^2 e^4}{m_0(v^2/Z)} L(x). \quad (2)$$

In these equations, Z and z are the charges of the stopping nuclei and the particle, respectively; e and m_0 are the electronic charge and rest mass; N is the number of stopping atoms per cm³; v and v_0 are the velocities of the particle and of the hydrogen electron, respectively; I is the mean ionization-excitation potential of the absorber, defined by Eq. (1); and ϵ is the atomic stopping cross section.

The present experiments were designed partly to provide accurate energy-loss data for comparison with these theoretical treatments of velocity region II by measuring the stopping cross sections of low-energy tritons in absorbers covering a wide range of Z's and, hence, a wide range of orbital electron velocities. The

* This work is based upon a thesis submitted by one of the authors (W.N.B.) to the Graduate School of the University of Florida in partial fulfillment of the requirements for the Ph.D. degree.

† Present address: This work was begun while R.L.W. was a staff member at the University of Florida.

‡ Present address: Hot Laboratory, Brookhaven National Laboratory, Upton, N. Y.

|| Operated by the Union Carbide Corporation for the U. S. Atomic Energy Commission.

[1] H. A. Bethe, Ann. Phys. (New York) **5**, 325 (1930).

[2] M. S. Livingston and H. A. Bethe, Rev. Mod. Phys. **9**, 245 (1937).

[3] H. A. Bethe and J. Ashkin, in *Experimental Nuclear Physics*, edited by E. Segrè (John Wiley & Sons, Inc., New York, 1953), Vol. 1, Part II.

[4] J. Lindhard and M. Scharff, Phys. Rev. **124**, 128 (1961).

[5] L. M. Brown, Phys. Rev. **79**, 297 (1950); M. C. Walske, *ibid.* **88**, 1283 (1952).

[6] M. C. Walske, Phys. Rev. **101**, 940 (1956).

[7] H. Bichsel, Bull. Am. Phys. Soc. **6**, 46 (1961); H. Bichsel, University of Southern California Linear Accelerator Group Technical Reports, Nos. 2 and 3, 1961 (unpublished).

[8] J. Lindhard and M. Scharff, Kgl. Danske Videnskab. Selskab, Mat.-Fys. Medd. **27**, No. 15 (1953).

energy of a triton having the same velocity as the hydrogen electron is 0.076 MeV; the energy of a triton having the same velocity as the K electrons in nitrogen, the lightest elementary absorber chosen for the present work, is 3.7 MeV. Thus, the present measurements of triton stopping cross sections from 2.7 MeV down to about 0.2 MeV fall mostly within region II as defined above, although region I is entered at triton energies below ~0.5 MeV.

The use of tritons as the penetrating particles has several advantages. According to theory,[1-8] the stopping cross section in a given material should be similar for all particles of the same charge and velocity; energy loss measurements on particles with $Z=1$ can, therefore, be done most accurately with tritons, since they have the greatest energy in any velocity region of interest. Nevertheless, no detailed studies of the stopping of low-energy tritons have been previously published, and only two measurements of the range of 2.7-MeV tritons in air are available.[9,10] Moreover, the currently growing interest in the acceleration of tritons for nuclear reaction studies makes it desirable to have accurate range-energy information for these particles in air, window materials, and targets.

In the present work, tritons of accurately known energy (2.736 MeV) were produced by the $Li^6(n,\alpha)H^3$ reaction and ranges and stopping cross sections were measured by a coincidence counting technique down to about 0.15 MeV in polystyrene, N_2, air, Al, Ar, Ni, Kr, and Xe.

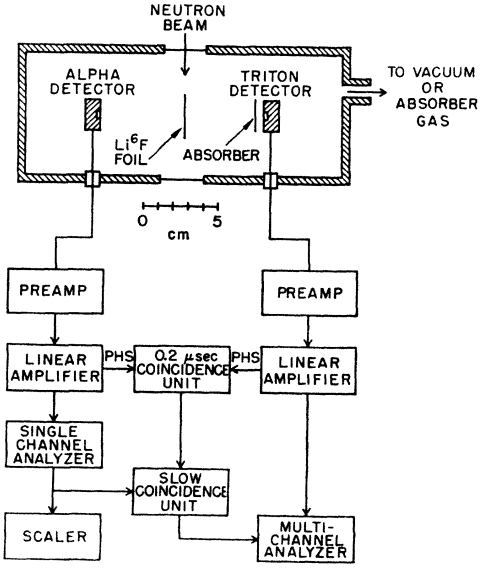

FIG. 1. Experimental arrangement.

[9] J. K. Bøggild and L. Minnhagen, Phys. Rev. **75**, 782 (1949).
[10] P. N. Cooper, V. S. Crocker, and J. Walker, Proc. Phys. Soc. (London) **66**, 600 (1953).

II. EXPERIMENTAL ARRANGEMENT

A collimated beam of thermal neutrons from the ORNL Low Intensity Test Reactor was directed at a 100 $\mu g/cm^2$ foil of evaporated Li^6F on a Formvar backing. The 2.736-MeV tritons and 2.052-MeV alpha particles which are produced at 180° to one another by the $Li^6(n,\alpha)H^3$ reaction were counted in 180° coincidence by two silicon surface-barrier detectors,[11] one on either side of the Li^6F target foil. The tritons were made to traverse various amounts of interposed absorber before entering the triton detector; they were then unambiguously identified by demanding coincidence with a 2.05-MeV alpha pulse in the alpha detector, as selected by a single-channel pulse-height analyzer. In this way, triton energy spectra relatively free of background effects were collected as a function of absorber thickness.

The experimental arrangement is shown schematically in Fig. 1. The neutron beam was collimated to 1 in. in diameter and entered a chamber containing the target, detectors, and absorber through an Al foil entrance window. After passing through the Li^6F target, the beam traversed the exit window and a 30-ft evacuated pipe to a borated paraffin beam stopper.

One-in. disks of the solid triton absorbers (polystyrene, Al, and Ni) were punched from commercial foils and weighed to determine their thicknesses. Various equivalent thickness of the gaseous absorbers (N_2, air, Ar, Kr, and Xe) were selected by filling the entire chamber to known pressures and calculating the equivalent thicknesses in mg/cm^2 from the measured temperatures, pressures, and distance between the target and the triton detector (68 mm). Since this procedure also interposed the gas between the target and the alpha-particle detector, the latter was moved closer to the target (5 mm instead of 68 mm) during the gaseous runs so that the gas thickness traversed by the alphas was less than their range even at the highest pressures used (about 1 atmos).

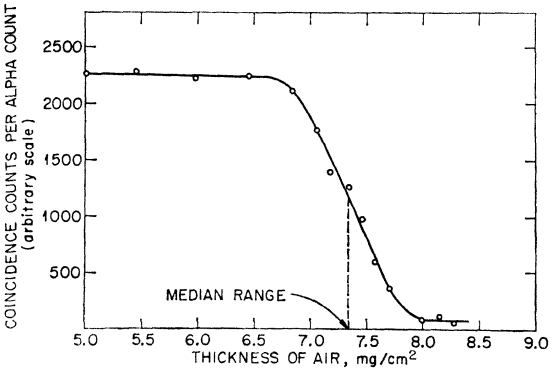

FIG. 2. Range curve of 2.736-MeV tritons in air.

[11] Detectors with 16 mm^2 active area were generously supplied by J. L. Blankenship and C. E. Ryan of the Oak Ridge National Laboratory Instrumentation and Controls Division.

The linearly amplified signals from the triton detector were applied to the input of a multichannel analyzer, which was gated by the pulses from the alpha detector by means of the coincidence arrangement shown in Fig. 1.

III. TREATMENT OF DATA

For each absorber thickness a triton coincidence spectrum was collected and fitted to a Gaussian shape of appropriate width to determine the peak position, which was then converted to energy. Energy calibration was accomplished by taking spectra of the undegraded $Li^6(n,\alpha)H^3$ tritons and alphas. The linearity of the system was further checked by measuring the pulse-height spectrum of 5.80-MeV Cm^{244} alpha particles as a function of air pressure in the chamber. From Bethe's critically compiled alpha-particle range-energy curve,[12] residual energies were calculated for each gas pressure and plotted against pulse height. The resulting plot was linear with a zero energy intercept; the measured range of 4.42±0.04 cm was in agreement with the value of 4.40±0.04 cm from Bethe's curve.

The median ranges of 2.736-MeV tritons were determined from plots of the number of α-t coincidences per alpha count vs absorber thickness. A typical curve is shown in Fig. 2. The median range was taken as the thickness which transmitted one-half the initial intensity of tritons.

Energy-loss values were derived as a function of absorber thickness by dividing the difference between the mean triton energies transmitted by two absorber thicknesses by the difference between the two thicknesses: $(E_1-E_2)/(x_2-x_1)=-\Delta E/\Delta x\approx -dE/dx$. In order to obtain accurate values of $\Delta E/\Delta x$ from the closely-spaced absorber measurements, the subtractions were done between pairs of points differing by ~200 keV, each experimental point being used only once as the initial and once as the final value in the subtractions. Each resultant value of $-\Delta E/\Delta x$ was plotted as $-dE/dx$ at the midpoint of its energy interval. From the analysis by Chilton, Cooper, and Harris,[13] it can be shown that for 200-keV intervals this approximation leads to an error in the energy scale of the $-dE/dx$ vs E plot which is smaller than the estimated error in determining the mean triton energies from the experimental spectra (~8 keV).

Range-energy curves were constructed by using the relation $R(E)=R(2.7)-x(2.7\rightarrow E)$, where $R(E)$ is the range of tritons of energy E, $R(2.7)$ is the measured range of the undegraded tritons, and $x(2.7\rightarrow E)$ is the absorber thickness required to degrade the tritons from 2.736 MeV to a mean energy E.

TABLE I. Median ranges of 2.736-MeV tritons.

Absorber	Range (mg/cm²)
Polystyrene	6.12±0.10
Nitrogen	7.26±0.06
Air	7.34±0.06
Aluminum	10.10±0.10
Argon	11.40±0.09
Nickel	15.15±0.15
Krypton	17.83±0.18
Xenon	20.36±0.20

TABLE II. Estimated contributions to error in the ranges of 2.736-MeV tritons.

Factor	Estimated error, Percentage of range
Thickness at half-point of counting rate	±0.75
Energy loss of tritons in source foil	−0.05
Energy loss in gold layer of detector	−0.01
Surface density of foils[a]	±0.2–0.5
Nonuniformity of foils[a]	±0.60
Distance between source and detector[b]	±0.5
Gas pressure[b]	±0.05
Gas temperature[b]	±0.05
Total error (solid absorbers)	±1.0–1.1
Total error (gaseous absorbers)	±0.9

[a] Solid absorbers only.
[b] Gaseous absorbers only.

IV. RESULTS AND DISCUSSION

The measured median ranges of 2.736-MeV tritons in eight stopping materials are given in Table I, in which the errors are based on the estimates shown in Table II. The only previously reported range measurements for 2.736-MeV tritons are in air. The values of[9] 7.36±0.07 and[10] 7.32±0.06 mg/cm² are in excellent agreement with our result, 7.34±0.06. The range-energy curves obtained from the present data are plotted in Fig. 3. Estimated errors in the range values are ~1%

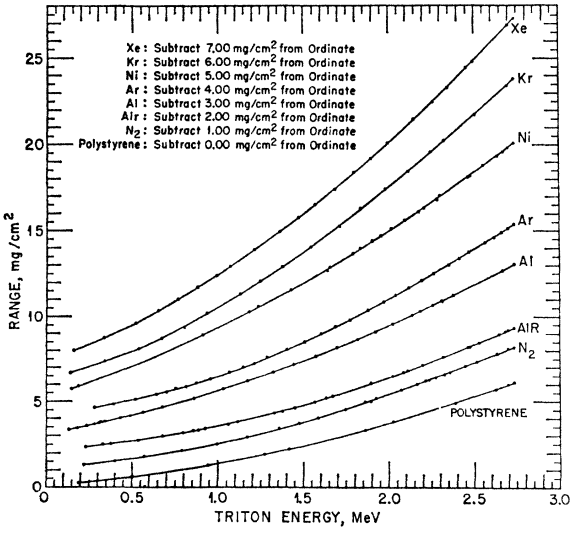

FIG. 3. Range-energy curves of tritons in various materials.

[12] H. A. Bethe, Rev. Mod. Phys. 22, 213 (1950).
[13] A. B. Chilton, J. N. Cooper, and J. C. Harris, Phys. Rev. 93, 413 (1954).

TABLE III. Atomic stopping cross sections for tritons.

Nitrogen		Aluminum		Argon		Nickel		Krypton		Xenon	
E (MeV)	$\epsilon\times10^{15}$ (eV-cm^2)	E (MeV)	$\epsilon\times10^{15}$ (eV-cm^2)	E (MeV)	$\epsilon\times10^{15}$ (eV-cm^2)	E (MeV)	$\epsilon\times10^{15}$ (eV-cm^2)	E (MeV)	$\epsilon\times10^{15}$ (eV-cm^2)	E (MeV)	$\epsilon\times10^{15}$ (eV-cm^2)
2.686	5.74	2.698	8.5	2.680	10.6	2.704	13.2	2.718	15.0	2.718	20.1
2.385	5.88	2.520	8.8	2.440	11.3	2.537	13.4	2.605	15.5	2.580	20.7
2.298	6.10	2.352	9.2	2.200	11.8	2.317	14.2	2.380	16.4	2.404	21.6
2.158	6.29	2.249	9.6	2.082	12.3	2.076	14.9	2.120	16.9	2.304	21.8
1.998	6.56	2.150	9.7	1.962	12.6	1.920	15.6	1.921	17.9	2.020	23.7
1.835	7.04	1.924	10.1	1.785	13.2	1.755	16.1	1.665	19.0	1.745	25.1
1.670	7.60	1.761	10.9	1.504	14.7	1.725	16.2	1.465	20.0	1.525	27.7
1.474	8.21	1.640	11.0	1.350	15.7	1.585	16.7	1.195	22.6	1.420	28.3
1.266	8.84	1.508	11.6	1.110	17.1	1.545	17.0	1.039	24.0	1.183	31.6
1.010	10.1	1.253	12.3	0.911	19.9	1.410	17.6	0.745	27.9	0.943	35.1
0.898	11.8	1.105	13.0	0.761	22.5	1.225	18.6	0.610	30.3	0.830	36.2
0.685	13.4	0.952	14.0	0.670	23.9	1.030	19.5	0.468	33.6	0.594	40.6
0.403	17.0	0.700	15.9	0.460	29.0	0.824	20.8	0.442	36.5	0.433	46.7
0.315	17.4	0.531	17.2	0.270	33.4	0.585	22.7	0.248	39.6	0.263	51.2
0.163	16.8	0.528	18.2	0.072	26.6	0.430	25.0	0.073	28.3	0.082	35.5
0.050	13.6	0.451	17.9			0.350	25.4				
		0.235	20.3			0.170	24.4				
		0.145	19.8			0.060	19.5				
		0.050	16.3								

at 2.7 MeV, increasing to $\sim3\%$ at the lowest energies. The energy scale is accurate to an estimated ±8 keV.

Atomic stopping cross sections of the elementary absorbers and energy-loss values for polystyrene and air are tabulated as a function of triton energy in Tables III and IV and are plotted as the solid black circles in Figs. 4–7. The cross sections, defined as $\epsilon=-(dE/dx)/N$, are in units of eV-cm^2, N being the number of stopping atoms per cm^3. (The values of ϵ may be converted to keV per mg/cm^2 by multiplying by 6.02×10^{17}/at. wt). The curves in Figs. 4–7 are drawn through the experimental triton points. All the curves have the expected shape: they reach a maximum as the tritons enter region I because electron pickup decreases their average charge and hence their rate of energy loss. The triton velocities at maximum energy loss all occur at about 1.7 to 2.0 times the ground-state hydrogen electron velocity. From Allison's summary[14] of charge-distribution measurements on protons in this velocity region, it can be inferred that the tritons are approximately 20–30% neutralized at the energy-loss maxima we observe in N_2, air, and Ar.

TABLE IV. Energy loss in polystyrene and air.

Polystyrene		Air	
E (MeV)	$-dE/dx$ (keV/mg-cm^{-2})	E (MeV)	$-dE/dx$ (keV/mg-cm^{-2})
2.718	290	2.678	246
2.665	288	2.633	247
2.214	330	2.490	254
1.952	358	2.260	269
1.752	381	2.150	271
1.529	427	1.995	300
1.348	465	1.785	311
1.110	515	1.560	337
0.722	645	1.275	389
0.302	854	0.995	460
0.098	802	0.845	505
		0.690	563
		0.305	716
		0.280	749
		0.180	720
		0.067	546

For comparison, previous measurements of stopping cross sections for protons,[13,15–23] deuterons,[23] and alpha particles[24] have been included in Figs. 4–7 after conversion to equivalent triton stopping cross sections by taking $\epsilon_1/\epsilon_2=z_1^2/z_2^2$ for two different particles of the same velocity as prescribed by stopping theory for completely stripped particles. The agreement is seen to be good at the higher energies, where the particles are well into region II. In Ni, Al, and Xe, the agreement with certain previous measurements is significantly better than with others. As they enter region I, nonisotopic particles would be expected to capture electrons at different rates because of their different electron velocities, but no differences would be expected among protons, deuterons, and tritons, and even the low-velocity portions of their stopping cross-section curves should coincide. The disagreement between the present data and some of the earlier proton and deuteron measurements at low velocities (notably in Ar, N_2, Al, and

[14] S. K. Allison, Rev. Mod. Phys. **30**, 1137 (1958).
[15] P. K. Weyl, Phys. Rev. **91**, 289 (1953).
[16] H. K. Reynolds, D. N. F. Dunbar, W. A. Wenzel, and W. Whaling, Phys. Rev. **92**, 742 (1953).
[17] D. C. Lorents and E. J. Zimmerman, Phys. Rev. **113**, 1199 (1959).
[18] J. A. Phillips, Phys. Rev. **90**, 532 (1953).
[19] M. Bader, R. E. Pixley, F. S. Mozer, and W. Whaling, Phys. Rev. **103**, 32 (1956).
[20] G. M. Osetinskii, Suppl. No. 5 to Soviet J. Atomic Energy, 70, (1957).
[21] D. Kahn, Phys. Rev. **90**, 503 (1953).
[22] S. D. Warshaw, Phys. Rev. **76**, 1759 (1949).
[23] H. Wilcox, Phys. Rev. **74**, 1743 (1948).
[24] G. W. Gobeli, Phys. Rev. **103**, 275 (1956).

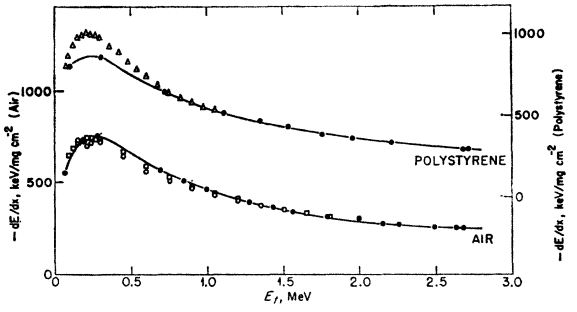

FIG. 4. Stopping cross sections in polystyrene and air. Proton, deuteron, and alpha-particle results in Figs. 4–7 have been converted to equivalent triton energy. (See text.) ●: tritons, present work. ○: protons, Weyl[15]; □: protons, Reynolds *et al.*[16]; △: protons, Lorents and Zimmerman.[17]

Ni) is probably due only to the greater experimental uncertainties in this region, although in this connection it may again be pointed out that tritons are the most

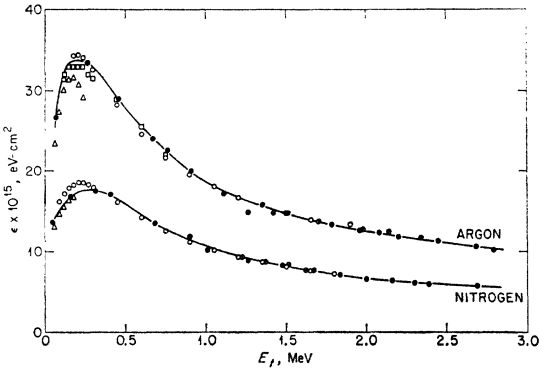

FIG. 5. Stopping cross sections in nitrogen and argon. ●: tritons, present work; ○ protons, Reynolds *et al.*[16]; △: protons, Phillips[18]; □: protons, Weyl[15]; ⊙: protons, Chilton *et al.*[13]

sensitive of the hydrogen-isotope particles for energy-loss measurements.

Although it depends heavily on a single experimental point, there appears to be a large difference between the

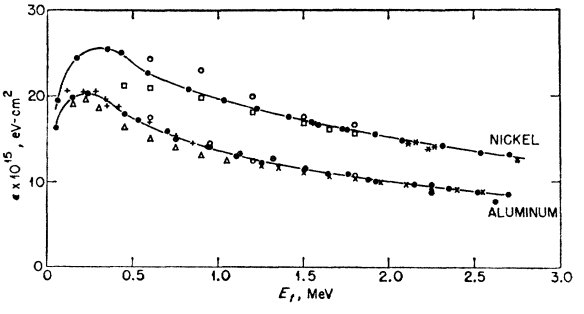

FIG. 6. Stopping cross sections in nickel and aluminum. ●: tritons, present work; ○: protons, Bader *et al.*[19]; □: protons, Osetinskii[20]; ⊙: alpha particles, Gobeli[24]; *: protons, Chilton *et al.*[13]; ×: protons, Kahn[21]; △: protons, Warshaw[22]; +: protons and deuterons, Wilcox.[23]

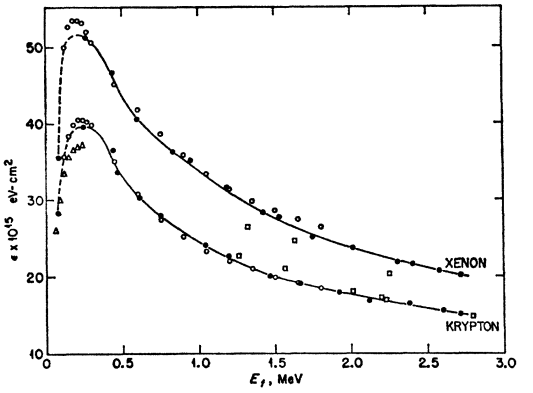

FIG. 7. Stopping cross sections in krypton and xenon. ●: tritons, present work; ○: protons, Reynolds *et al.*[16]; △: protons, Phillips[18]; □: protons, Chilton *et al.*[13]

proton and triton data as the particles approach region I in polystyrene (Fig. 4). The higher energy loss of the protons might be attributed to the absorber's large hydrogen content and/or to the possibly variable composition of the material.

The present data may be compared with two theoretical treatments of velocity region II. Lindhard and Scharff[8] have plotted experimental values of L from Eq. (2) against x to determine the function $L(x)$, which is presumed to be valid in and above region II for all elementary absorbers. Figure 8 is a modified Lindhard-Scharff plot of the present data in which ϵ has been plotted directly instead of L and the variable $x=v^2/(v_0^2Z)$ has been replaced by E_t/Z, where E_t is the triton energy in MeV. (Conversion of the variable E_t/Z to Lindhard and Scharff's x is accomplished for tritons by multiplying by 13.2.) The data have been fitted by the function $\epsilon\times10^{15}(\text{eV-cm}^2)=4(E_t/Z)^{-1/2}-(E_t/Z)^{1/2}$, which is of the same functional form as Lindhard and Scharff's $L(x)=1.36x^{1/2}-0.016x^{3/2}$ [since $L\propto\epsilon x$ from Eq. (2)], but differs in the constants. The fit is increasingly good at higher energies and increas-

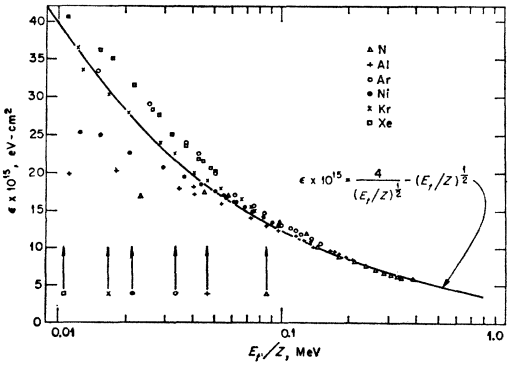

FIG. 8. Modified Lindhard-Scharff plot of present data. The points are experimental; the curve is the best equation having the functional dependence of Lindhard and Scharff's $L(x)$. The arrows at the bottom show the values of E_t/Z for a triton energy $E_t=0.6$ MeV.

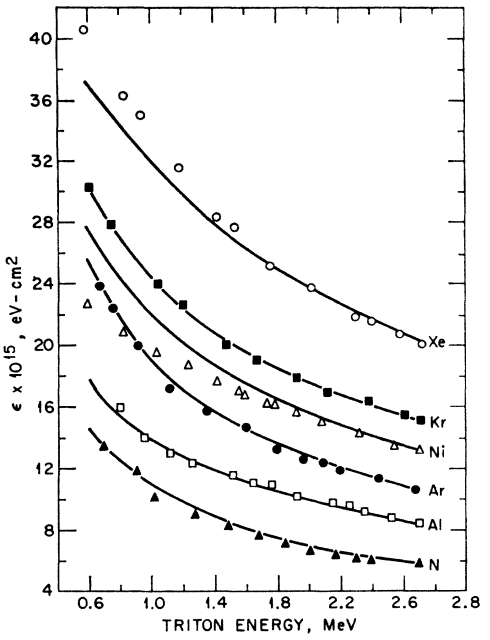

FIG. 9. Triton stopping cross sections compared with Bichsel's semiempirical shell correction calculations. The points are experimental; the curves are calculated.

ingly unsatisfactory as the tritons approach and enter region I. If the Lindhard-Scharff theory is expected to hold only above $E_t \approx 0.6$ (or $v \approx 3v_0$), the low-energy deviations may be ignored. As a guide, the value of E_t/Z for $E_t = 0.6$ MeV has been indicated near the bottom of Fig. 8 for each element. Above ~0.6 MeV, the data and theory are in approximate agreement for both solid and gaseous absorbers with the possible exception of xenon. At lower energies, the lack of agreement becomes evident for all cases except krypton.

Bichsel[7] chose an approach which applies all shell corrections in order to account for the data of region II. He assumed the M, N, O, etc., shell correction terms to be of the same functional dependence as the more easily calculated L-shell correction terms of Walske,[6] and maintained energy-independent ionization potentials. His calculations[25] for the present systems, using mean ionization-excitation potentials of 90.00, 163.00, 200.00, 310.00, 360.00, and 480.00 eV for N, Al, Ar, Ni, Kr, and Xe, respectively, are compared with the present data in Fig. 9. The agreement above ~0.6 MeV is excellent for N, Al, Ar, and Kr, but not for Ni and Xe. While no explanation for the disagreement in Xe (which was apparent to a greater extent in the Lindhard-Scharff comparison) is immediately apparent, it may be that the assumed similarity of the higher correction terms to the L-shell terms is invalidated by the incomplete inne electron configuration of the transition metals. It is to be noted that nickel is relatively well behaved in the Lindhard-Scharff plot of Fig. 8.

In summary, it appears that both the Lindhard-Scharff theory and the Bichsel semiempirical method are in general agreement with the present data. The Lindhard-Scharff treatment is increasingly successful at higher energies; the validity of the Bichsel treatment does not seem to be as strongly energy dependent, extending further down toward region I, but it appears to be sensitive to the details of the stopping medium's electronic configuration.

ACKNOWLEDGMENTS

We express our thanks to Dr. H. Bichsel for his calculation of the shell correction terms for our experimental systems. We also wish to acknowledge the assistance of the Reactor Operations Department of the Oak Ridge National Laboratory and the operating staff of the Low Intensity Test Reactor. One of us (W.N.B.) is grateful to the Oak Ridge Institute of Nuclear Studies for a Graduate Fellowship.

[25] H. Bichsel (private communication).